Prospects of Open-Charm Asymmetry Measurements at the SPD

Amaresh Datta
JINR, DNLP
Dubna, Russia

Contents

Abstract

The Spin Physics Detector (SPD) at the Nuclotron based Ion Collider fAcility (NICA) is designed to study nucleon spin structure in the three dimensions. With capabilities to collide polarized protons (up to $\sqrt{s} = 27$ GeV) with peak design luminosity 10^{32}cm^{-2} s^{-1}, the experiment will allow measurements of cross-sections and spin asymmetries sensitive to the unpolarized and various polarized gluon distributions inside the nucleons. In the kinematic regime to be probed by the SPD, the leading mechanism of charmed D meson productions in proton-proton collisions are dominated by the interactions involving gluons. This work presents methodology of the detection of charmed D mesons via their hadronic decay channels. It also studies the precision of transverse single spin asymmetry (TSSA) measurements and their impacts on the current models describing gluon TMD distribution such as Gluon Sivers Function (GSF).

1 Introduction

At SPD energies gluon fusion process dominates charm meson production. About 70% of the charm meson production are generated by the gluon-gluon scattering. This makes the charm meson (i.e. $D^0, \bar{D^0}, D^{\pm}$) asymmetries sensitive to the gluon spin distributions. It is the third probe of particular interest besides direct photon and charmonia at the SPD in stage II physics program probing gluon distributions in general.

SPD will attempt to measure charm mesons via their hadronic decay channels

- $D^0 \to \pi^+ + K^-$, $\bar{D}^0 \to \pi^- + K^+$
- Branching Ratio 3.89%, $c\tau = 0.41$ ps, $\lambda = 123$ μm
- $D^+ \to \pi^+ + \pi^+ + K^-$, $D^- \to \pi^- + \pi^- + K^+$
- Branching Ratio 9.22%, $c\tau = 1.04$ ps, $\lambda = 312$ μm

2 Vertex Detector Options

As of early 2024, the design of vertex detector for the stage II physics is not decided. Possible options are :

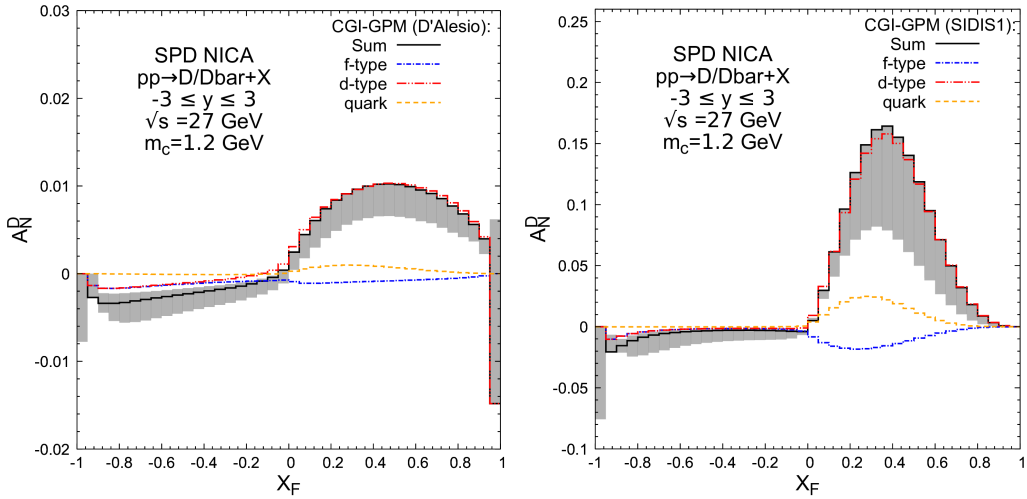

(a) D'Alesio parameters for gluon Sivers function (GSF).

(b) D'Alesio parameters for gluon Sivers function (GSF).

Figure 1: Theoretical estimations of inclusive D meson TSSA.

- MicroMegas typically for the stage I physics, however this might be the retained for stage II in case better SVD is not available
- DSSD (Double Sided Silicon Detector) based SVD, quite good, probably with both barrel and end-caps
- MAPS (Monolithic Active Pixel Sensor) based SVD (silicon vertex detector), possibly the best option, probably barrel only

In the current TDR (technical design report), proposed MicroMegas (Fig:2a) is one super layer (containing three sub layers) with a total thickness of $\sim$ 1120 μm, z-length of 90 cm and the material thickness corresponds to $3 \times 0.4\%$ of radiation length of Si (9.37 cm).

DSSD, according to TDR (Fig:2b) consists of three layers with both barrel and end-cap parts. Barrel z-length is 74 cm and the layer thickness of 500 μm accounts for 0.53% of radiation length in Si.

MAPS based SVD, according to the current TDR (Fig:3a) consists of 4 layers of only barrel part with z-length 150 cm and layer thickness 750 μm corresponding to 0.8% of radiation length in Si.

We also consider a second possible configuration (Fig:3b) of the MAPS based SVD, with less thickness, shorter barrel part and including end-caps.

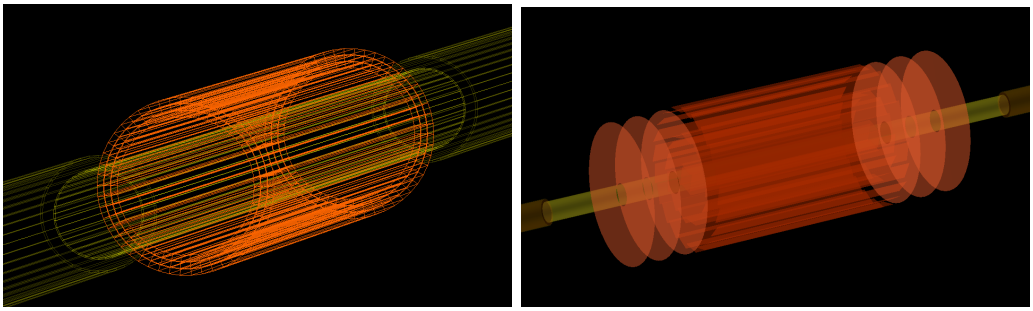

(a) MicroMegas - TDR configuration. (b) DSSD - TDR configuration.

Figure 2: Possible Silicon vertex Detector (SVD) configurations for stage II.

This version has layer thickness 335 μm that corresponds to 0.35% of radiation length in Si.

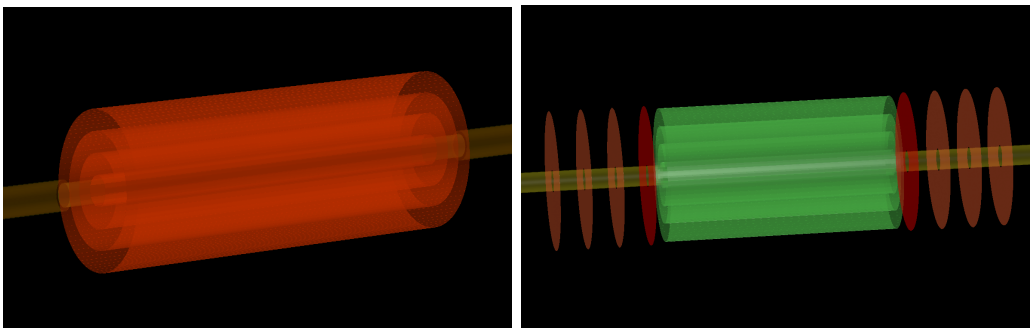

(a) MAPS - TDR configuration (b) MAPS - 'wish-list' configuration

Figure 3: Possible Silicon vertex Detector (SVD) configurations for stage II..

As will be demonstrated here, MAPS based SVD is decidedly more accurate in secondary vertex reconstruction that is crucial in D meson detection at the SPD. So, we consider another configuration of MAPS based SVD - a sort of 'wish-list' configuration - with four layers including end-caps and shortened barrel part similar to DSSD ($\sim$ 74 cm).

We studied performance of these SVD setups using neutral D meson simulations and studying its decay via hadronic channel $D^0 \longrightarrow \pi^+ K^-$ for the purpose of reconstructing the decay of the D^0 meson produced from $p + p$ collision at $\sqrt{27}$ GeV, as is expected in the final stage of the SPD.

PYTHIA8 was used as even generator. Detector GEANT4 description

and CERN Root based reconstruction software SpdRoot was used for studying the output. Event vertex profile was assumed to be Gaussian along the beam (z) direction with a width of 30 cm. Kalman filter based software KFParticle package (part of SpdRoot) was used to reconstruct event vertex form possible daughter candidate tracks.

2.1 Spatial Resolutions of Secondary Vertex Reconstruction

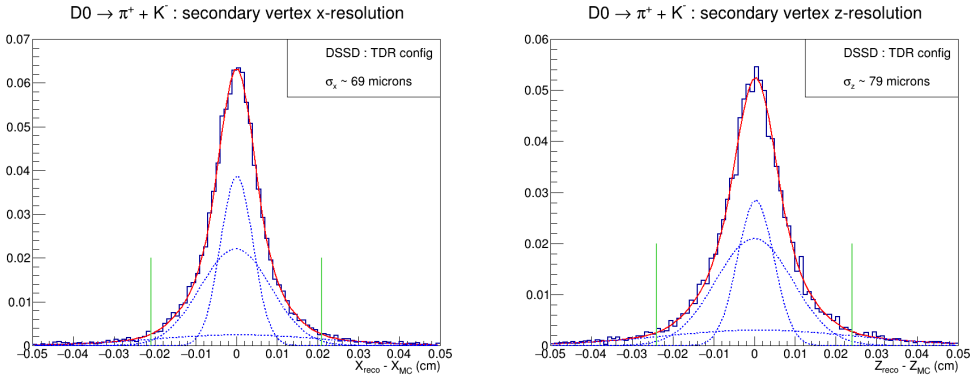

(a) X-direction. (b) Z-direction.

Figure 4: DSSD (TDR) : secondary vertex resolutions.

Spatial resolution of the secondary vertex reconstruction in beam(z) and perpendicular(x) direction are shown here (Figs:4,5,6). Histograms shown here represent the difference between the true MC generation point of daughter particles from a D^0 decay and the position of the secondary vertex as reconstructed by the KFParticle package.

Histograms are fitted with three Gaussians. Widest Gaussian is very wide and has very small peak value, behaving almost like a flat background/noise and is ignored for effective resolution calculation. The effective resolution is calculated (3σ ranges are shown on plots with vertical lines) as weighted average of the two narrow Gaussians.

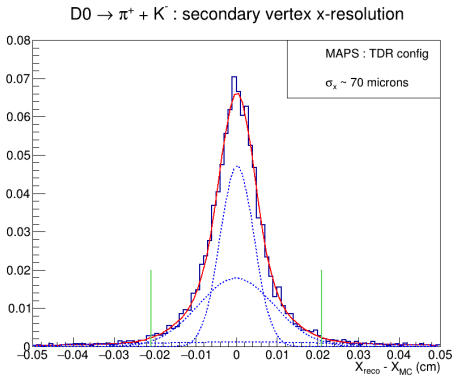

(a) X-direction.

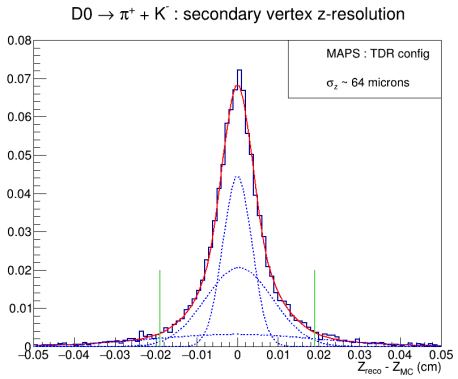

(b) Z-direction.

Figure 5: MAPS (TDR) : secondary vertex resolutions.

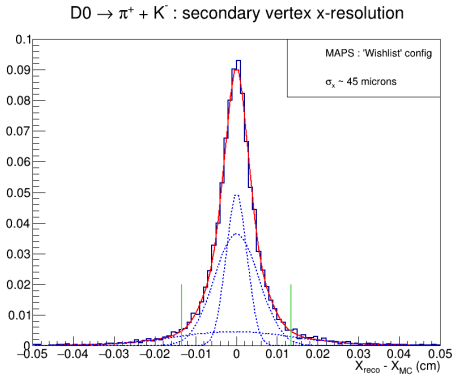

(a) X-direction.

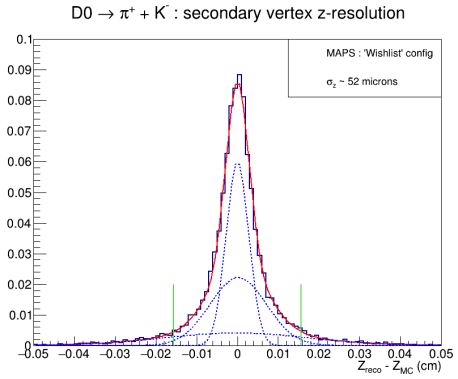

(b) Z-direction.

Figure 6: MAPS ('wish-list') : secondary vertex resolutions.

2.1.1 Comparison of Resolutions

Spatial resolutions of secondary vertex reconstruction using different versions of the SVD are compared below for both X and Z directions. As the plots show (Fig:7) that MicroMegas has resolutions $\sim$ 300 μm, almost 3 times as large as the decay length (120 μm) of D^0 and of the same size as that (310 μm) of the charged D meson. It is, therefore, of limited use for stage II physics, in particular for D meson asymmetry and cross-section measurements.

In the z-direction, MAPS shows $\sim$ 20% better resolution compared to DSSD (Fig:7b), both as described in the TDR.

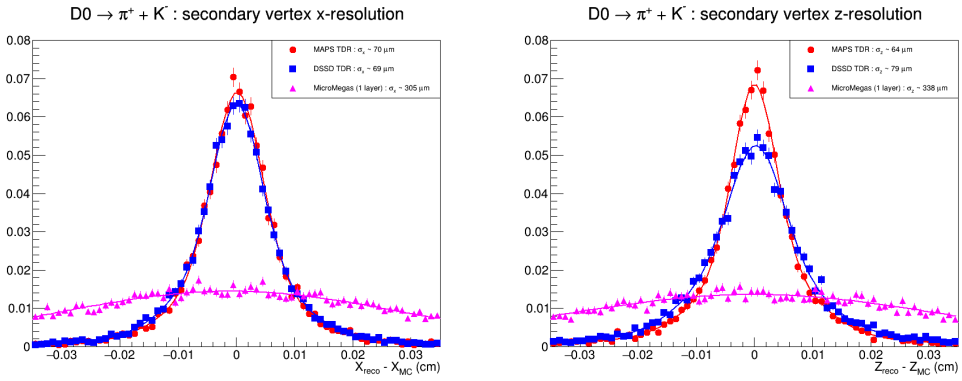

(a) X-direction. (b) Z-direction.

Figure 7: Comparison of secondary vertex resolutions of TRD configurations.

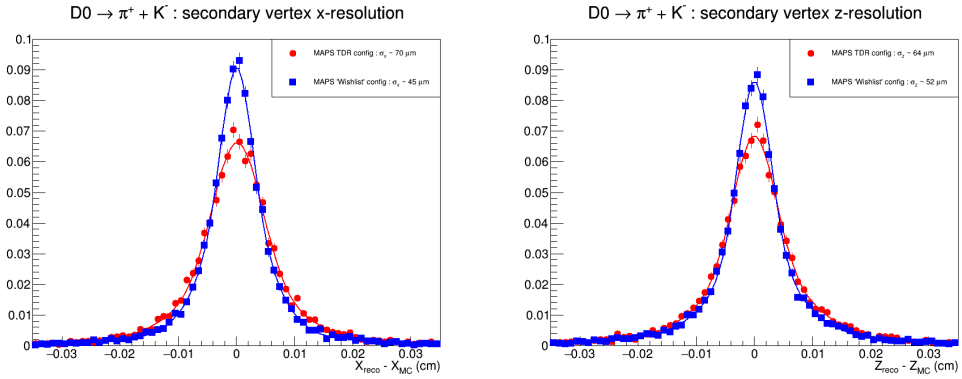

(a) X-direction. (b) Z-direction.

Figure 8: Comparison of secondary vertex resolutions of two different MAPS configurations.

We also compare the performances of the two different configurations of the MAPS based SVD. The 'wish-list' configuration shows (Fig:8b) significantly ($\sim 20\%$) better resolution.

The non-TDR configuration of the MAPS based SVD is also of particular interest because, like the TDR version of the DSSD, it includes end-caps. For the D meson Transverse Single Spin Asymmetry (A_N) measurements, large asymmetries are expected from the high positive x_F kinematic regions and the presence of end-caps demonstrably (Fig:9) increases statistics in the high

x_F region. This is important for making an A_N measurement with small enough statistical uncertainty to be able to distinguish between competing models of Gluon Sivers Function (GSF) i.e. SIDIS and D'Alesio parameter sets.

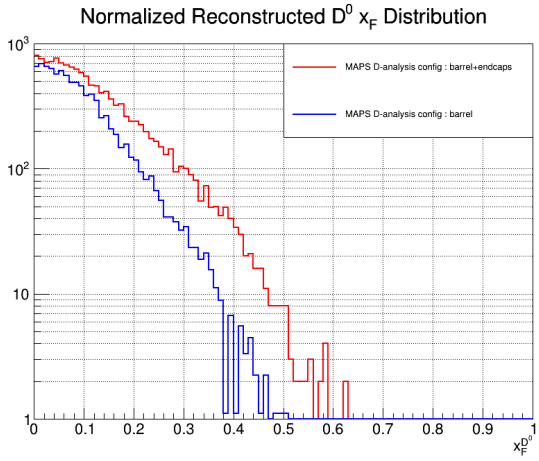

Figure 9: Reconstructed $x_F^{D^0}$ with and without MAPS end-caps.

3 Simulation Details

The analysis looked into multiple detector setups with different versions of inner tracker/silicon vertex detector and also various levels of 'realistic' simulation i.e. events generated at nominal collision center (0,0,0) vs Gaussian vertex profile with 30 cm width, ideal particle identification vs. PID from Time-of-Flight (TOF) detector etc.

3.1 Ideal Simulation

First, we present results of ideal simulations with events generated at nominal collision center (0,0,0) and perfect particle identification (using MC information). Two sets of events were generated. Four million open-charm events were generated and D^0 mesons are forced into decay channel of interest ($D^0 \longrightarrow \pi^+ K^-$) to study the signal for the intended measurement. In addition, forty million minimum bias events (excepting elastic) were generated to study the background to the measurement which arise from random combinations of pions and kaons created not from D meson decay but from other hard processes.

- Detector subsystems switched on for the simulation are : (beryllium) beam-pipe, inner tracker/vertex detector, straw tracker and magnet
- Magnetic field : $B_z = 1$ T
- MAPS based 'wish-list' SVD was used
- Pion and kaon tracks to reconstruct secondary vertex were selected to have converged fit and with at least three hits in the SVD
- V_0 or decay vertices were reconstructed with KFParticle package using KFParticle objects of the daughter track candidates
- In signal events, random combinations are ignored for the time being (separate small scale study demonstrated the effect is negligible compared to the background from minimum bias events)
- SpdVertexCombiFinder (a class in SpdRoot software) was used to reconstruct all possible combinations of (π, K) in background/min-bias events

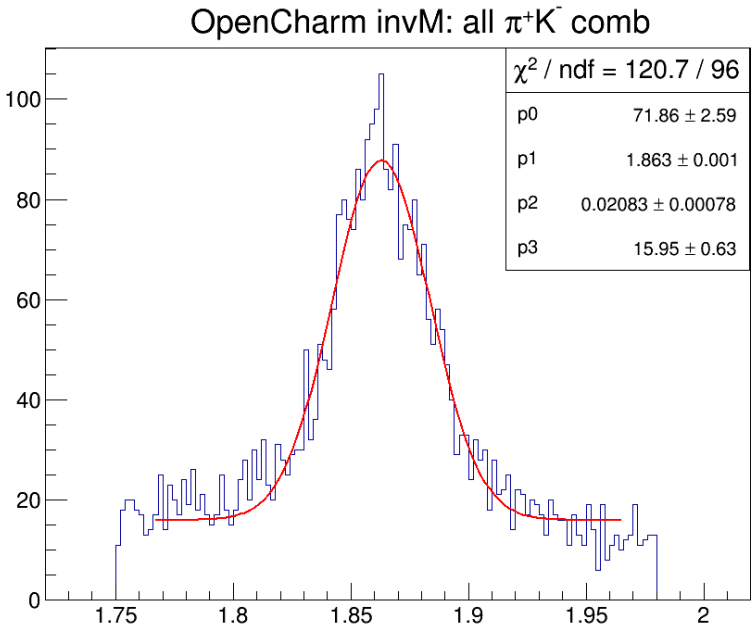

Figure 10: All possible π^+K^- combinations from open-charm events.

3.1.1 Random Background in Signal Events

A small scale simulation study with open-charm events only were performed to study the quantitative scale of random (π^+K^-) background from events containing D mesons. The results (Fig:10) shows the presence of combinatorial background and such background is of the order of $10-15\%$ of the signal counts, which is negligible compared to the 4-5 orders of magnitude higher combinatorial background arising form the min-bias events. This study, therefore, neglects this source of background in the subsequent parts.

3.2 Realistic Simulation

In contrast to the ideal simulation, a more realistic simulation differs in two crucial aspects : 1) event vertices are generated as Gaussian shapes in three dimensions ($\sigma_{x,y} = 0.1$ cm, $\sigma_z = 30$ cm) and 2) realistic charged particle identification. For particle identification, TOF likelihoods are used up to 1.5 GeV/c momentum of tracks with PID corresponding to the maximum

likelihood is assigned to the track. Beyond 1.5 GeV/c momentum, threshold Aerogel information is used to distinguish between pions and kaons. Both these methods of course introduce impurities and possibly widens the invariant mass distribution of the signal.

As a side note, FARICH detector might be very helpful in assigning PID more accurately. Also presentation from Alexander Ayriyan (Jan 24, 2024 Physics and MC Meeting) demonstrated (with MPD data) that gradient boosted decision tree combining information from SVD and ST and ToF (momentum, energy loss, mass-squared) can predict PID with high accuracy. So, hopefully one or both of these hardware and software solutions will provide us with high precision and high efficiency PID determination of charged tracks in the final analysis.

4 Signal Asymmetry and Uncertainty

Typically for asymmetry calculation (as can be found in analyses from any of the similar experiments like STAR, PHENIX, COMPASS) of a signal peak with some background underneath, the asymmetry is a combination of that of both the signal and the background. Background asymmetry is separately estimated from background dominated region in the spectrum (of invariant mass in detection of decay events) and subtracted statistically to obtain the desired signal asymmetry.

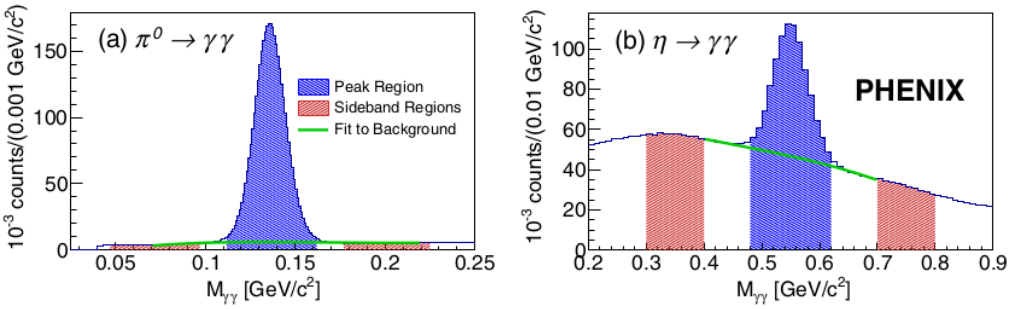

(a) Invariant mass spectra for $\pi^0 \longrightarrow \gamma\gamma$ at PHENIX.

(b) Invariant mass spectra for $\eta \longrightarrow \gamma\gamma$ at PHENIX.

Figure 11: Example of asymmetry measurement and correction for the background.

As is illustrated in the examples (Fig:11a and Fig:11b) of invariant mass spectra for di-photons for detecting η and π^0 mesons at the PHENIX experiment, particle candidates are counted both in the peak region (typically in a 2σ range), indicated on the plots by blue band. This 'raw' count includes signal as well as some (combinatorial) background candidates. As the plots show, (almost) pure background counts are counted from the regions - indicated by the (red bands) on both sides of the signal peak - dominated by background and at least 3σ away from the signal peak position.

These counts for two separate polarization of the beam are used to calculate asymmetries (let's say TSSA : A_N^{raw}, A_N^{bkg}) and their statistical uncertainties ($\sigma_{A_N}^{raw}, \sigma_{A_N}^{bkg}$) for the 'raw' and 'background' counts separately. Then the raw asymmetry and its statistical uncertainty are corrected using background asymmetry, its uncertainty and the relative ratio ($r = \frac{N_{bkg}}{N_{raw}}$) of the background to the total count in the blue band.

$$A_N(\phi) = \frac{1}{P\langle|cos(\phi)|\rangle} \frac{N(\phi) - \mathcal{R}.N(\phi+\pi)}{N(\phi) + \mathcal{R}.N(\phi+\pi)} \tag{1}$$

where P is beam polarization, $\langle|cos(\phi)|\rangle = \frac{\int_{\phi_1}^{\phi_2} cos(\phi) d\phi}{\phi_2 - \phi_1}$ is the average of the cosine of azimuth in the ϕ bin, $\mathcal{R}$ is relative luminosity for the two different polarizations of the beam, N's are counts in ϕ bins.

Statistical Uncertainty of TSSA (propagation of error assuming two independent variables $N(\phi)$ and $N(\phi+\pi)$) :

$$\sigma_{A_N}(\phi) = \frac{1}{P\langle|cos(\phi)|\rangle} \frac{2\mathcal{R}.N(\phi).N(\phi+\pi)}{(N(\phi) + \mathcal{R}N(\phi+\pi))^2} \sqrt{(\frac{\sigma_{N(\phi)}}{N(\phi)})^2 + (\frac{\sigma_{N(\phi+\pi)}}{N(\phi+\pi)})^2} \tag{2}$$

Assuming $\mathcal{R} \sim 1$, $N(\phi) \sim N(\phi+\pi) = N$ where N is the count of particle candidates in a ϕ bin ($N = N_{detected}/n$ with n bins in the azimuth) and assume Poisson distribution of counts (so that $\sigma_N = \sqrt{N}$), a simplified version of statistical uncertainty of TSSA can be written as:

$$\sigma_{A_N}(\phi) = \frac{1}{P\langle|cos(\phi)|\rangle} \frac{1}{\sqrt{2N}} \tag{3}$$

Now the signal asymmetry and its statistical uncertainty can be extracted as :

$$A_N^{Sig}(\phi) = \frac{A_N^{Raw}(\phi) - r.A_N^{Bkg}(\phi)}{1-r} \tag{4}$$

$$\sigma_{A_N^{Sig}}(\phi) = \frac{\sqrt{\sigma^2_{A_N^{Raw}}(\phi) + r^2\sigma^2_{A_N^{Bkg}}(\phi)}}{1-r} \tag{5}$$

4.1 Projected Statistical Uncertainty Calculation

In the simulated study, we can not estimate asymmetries since the event generators do not use polarized PDFs. We can, however, estimate statistical uncertainties for an expected amount of data (measured in integrated luminosity) from the count of selected particle candidate (D^0 mesons in this study). These uncertainties can be compared with theoretical expectations, especially if there are multiple estimations coming from various models of the (polarized) parton distributions and hadronization. Size of the expected statistical uncertainties can indicate whether a measurement will be able to distinguish between the different models.

As the study is limited in statistics, especially in the case of minimum bias background events, after the selection criteria are applied there are not enough counts of invariant mass spectra available for a proper fit to the signal and background. As a workaround, we scale simulated counts to those expected from one year of data.

First, the counts of D mesons from the open-charm events decaying into channel of interest are scaled to the number expected from one year of data (360 million D^0 and 520 million D^+ according to the CDR [1]). In a similar way, generated background events are scaled to the number of minimum bias events expected (32800 billion) in one year of data. These two factors are used to scale reconstructed counts of signal and background from simulation respectively to generate the expected invariant mass spectra for one year of data *before* any selection.

Next the ratio of counts of signal and background from the simulation study *before and after* the application of the selection criteria are used to estimate respective *suppression factors*. These factors are multiplied to the above mentioned scaled signal and background spectra (for one year data) to generate invariant mass spectra for one year of data *after* any selection.

The invariant mass spectra after the selection are fitted with typically a Gaussian signal and a linear background shape. From the fit, the nominal D meson mass and 2σ mass window and signal and background counts in this window are determined. Counts in individual x_F bins from the simulation are scaled to expected counts in one year of data. Raw (signal+background)

and background counts are subsequently used for the estimation of statistical uncertainties. The ratio $r = \frac{N_{bkg}}{N_{raw}}$ is used for the calculations.

Finally, for each x_F bin, counts N_{raw}, N_{bkg} are distributed uniformly in 12 ϕ bins. Raw and background statistical uncertainties $(\sigma^{raw}_{A_N}, \sigma^{bkg}_{A_N})$ are estimated for each ϕ bin. For each pair of $\phi, (\phi + \pi)$ (or left and right) bins, signal statistical uncertainty is extracted using $\sigma^{raw}_{A_N}, \sigma^{bkg}_{A_N}$ and r. Finally, independent measurements of uncertainties from six pairs of ϕ bins (left and right) are combined to estimate the statistical average :

$$\sigma_{A_N^{sig}}(x_F) = \frac{1}{\sqrt{\sum_{i=1}^{6} \frac{1}{\sigma^2_{A_N^{sig}(\phi_i)}}}} \tag{6}$$

This study will use this estimated statistical uncertainty of TSSA to compare with two different estimates of A_N^D as functions of Feynman-x from our Samara colleagues [2].

5 Results and Discussion

5.1 Neutral D Ideal Simulation with MAPS 'wish-list' SVD

Ideal simulation in particular uses two aspects that are ideal 1) all events are generated at nominal center of collision (0,0,0) and 2) assumed perfect PID for charged particles (daughter track candidates) from MC information.

A multitude of variable/quantities related to individual tracks and reconstruction of the secondary vertices are looked at to distinguish the behaviour of the signal D mesons and the combinatorial background.

Kinematic variables of the π^+K^- invariant particles are shown here but no selection criteria are applied based on these to retain the D meson distributions in Feynman-x (x_F) unbiased. Most of the selection criteria are related to the reconstruction of the secondary vertex. Decay length and its uncertainty, various χ^2 and distances ('distance of closest approach' or DCA) i.e. between daughter tracks, daughter track to primary vertex (PV) or secondary vertex (V0), between invariant particle to primary vertex etc. display various degrees of differentiating patterns of the signal and the background distributions.

Cuts are typically decided based on the inflexion point where signal starts dominating when the normalized distributions are compared with the aim to maximize signal-to-background in the selected sample. Events are counted before and after the application of selection criteria and in the entire x_F range as well as in $|x_F| \geq 0.2$ (aimed specifically for A_N measurements). Also all invariant mass distributions shown in this analysis are restricted to $1.7 \leq M_{inv} \leq 2.0$ GeV/c^2, that is, in a range roughly centered around the D meson mass ($M_{D^0} = 1.865$ GeV/c^2, $M_{D^+} = 1.870$ GeV/c^2).

Four million open-charm events and forty million minimum bias events were generated for this study. D^0 mesons were forced to decay in π^+K^- channel.

Full set of selection criteria used are listed below :

- Decay length : $L > 0.008$ cm, $L/\delta L > 2$.
- Collinearity angle : $Acol < 0.3$ rad
- V0 properties : $\chi^2_{V0-PV} > 0.5$, $DCA_{V0-PV} > 0.004$ cm
- Daughter track properties :
- $DCA_{\pi-K} < 0.01$ cm, opening angle $OA < 1.5$ rad
- Daughter to PV : $\chi^2_{d-PV} > 1.5$, $DCA_{d-PV} > 0.01$ cm
- Daughter to V0 : $DCA_{d-V0} < 0.005$ cm
- Invariant mass window 1.7-2.0 GeV/c^2
- $|x_F| > 0.2$ for asymmetry measurements

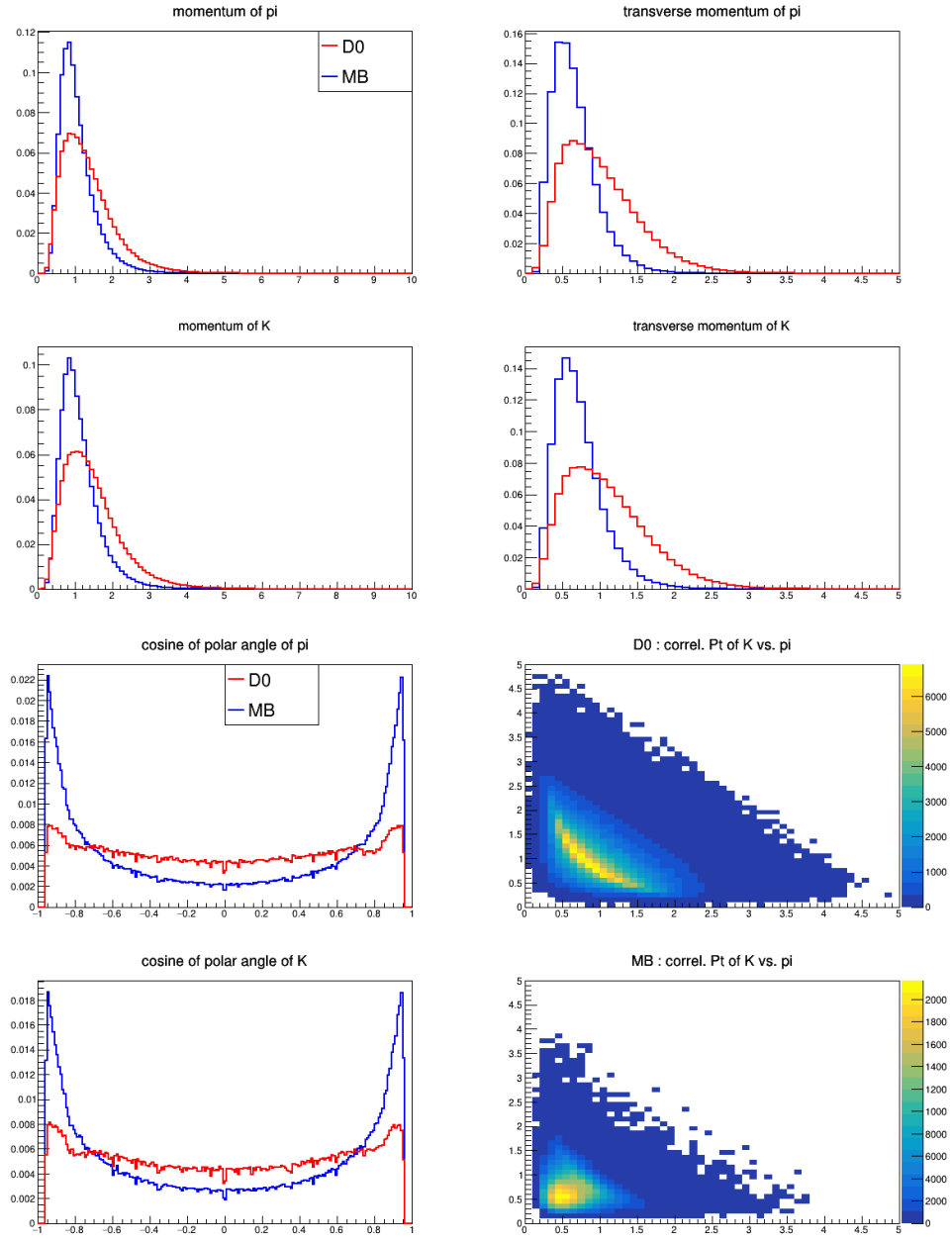

Figure 12: Kinematic properties of daughter track candidates. No cuts are applied to keep kinematic distribution of D^0 unbiased.

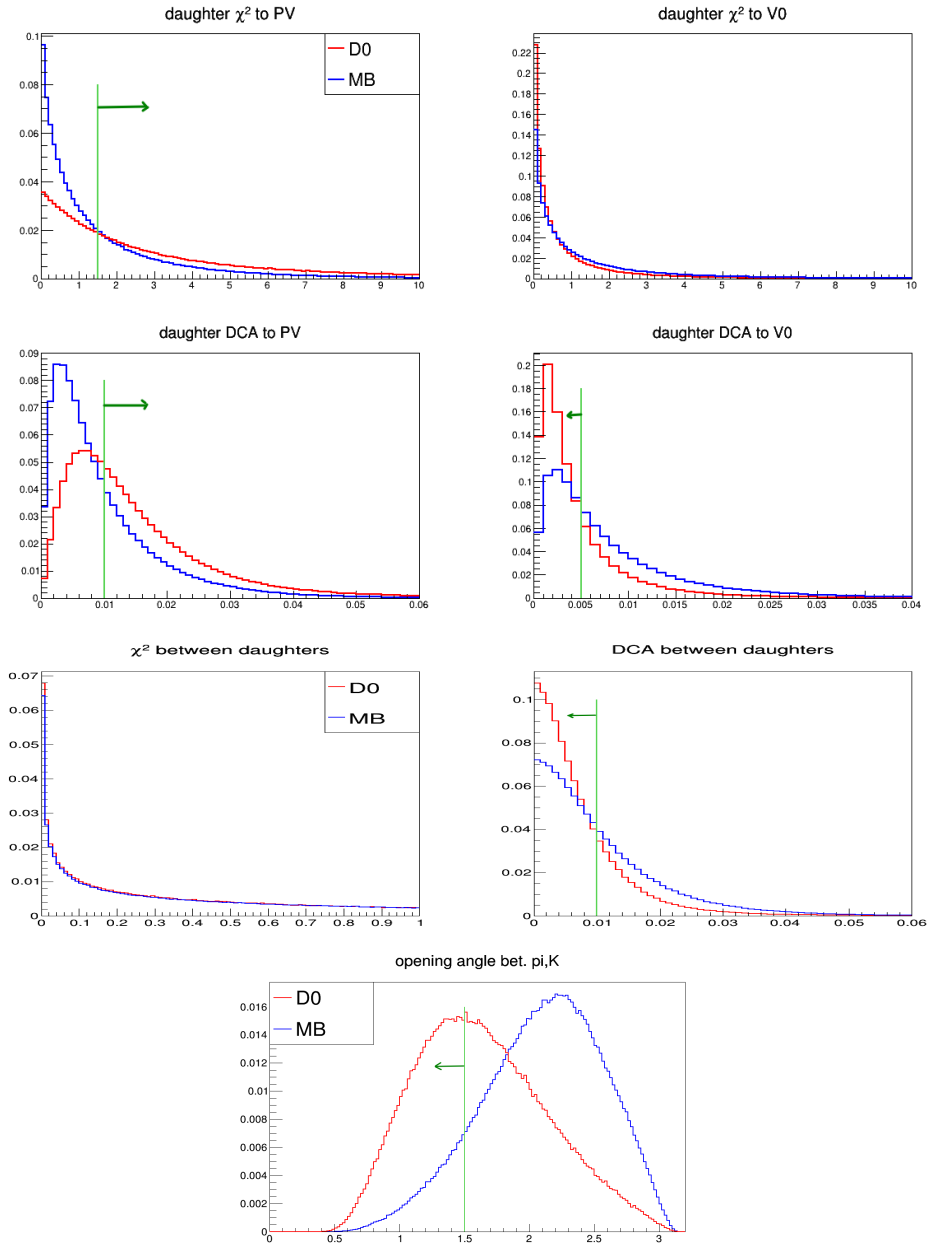

Figure 13: Properties of daughter track candidates. Cuts shown with green lines.

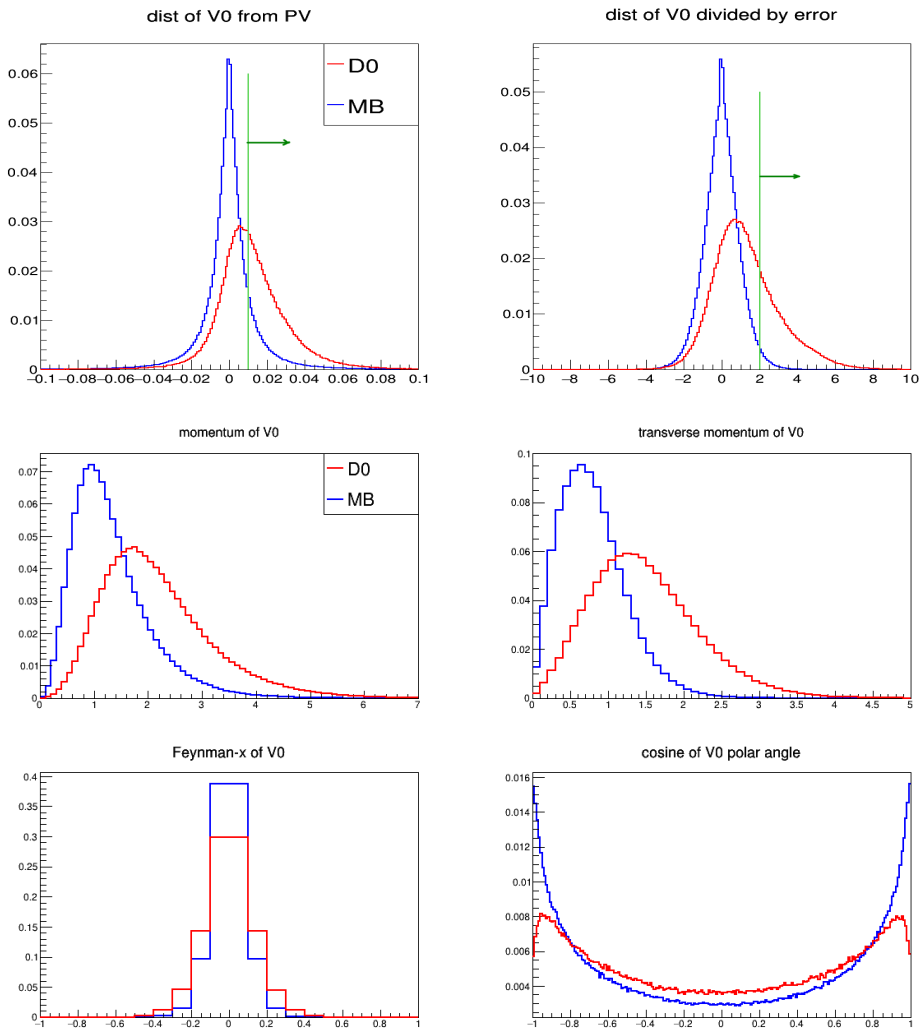

Figure 14: Properties of reconstructed invariant particle. Cuts shown with green lines.

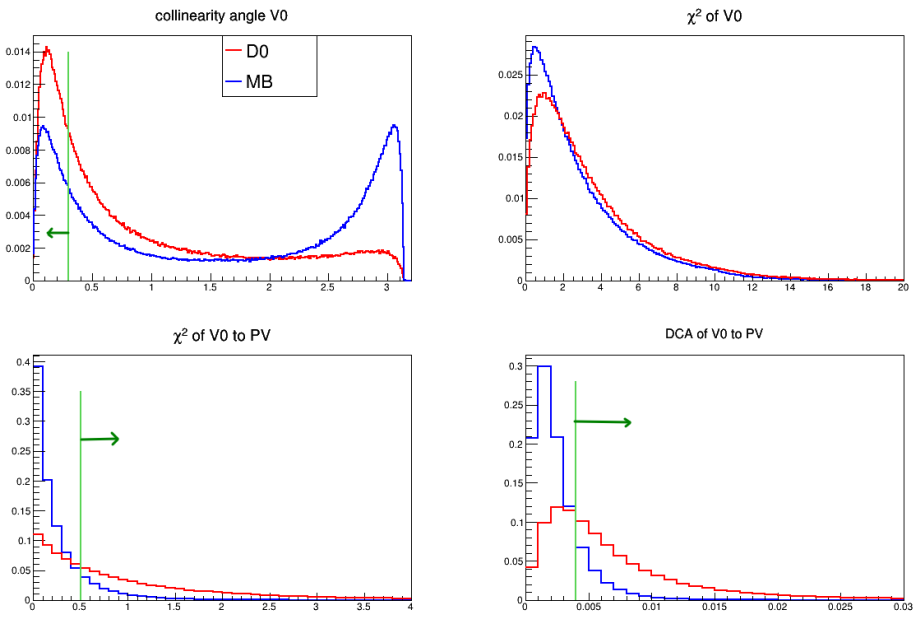

Figure 15: Properties of reconstructed invariant particle. Cuts shown with green lines.

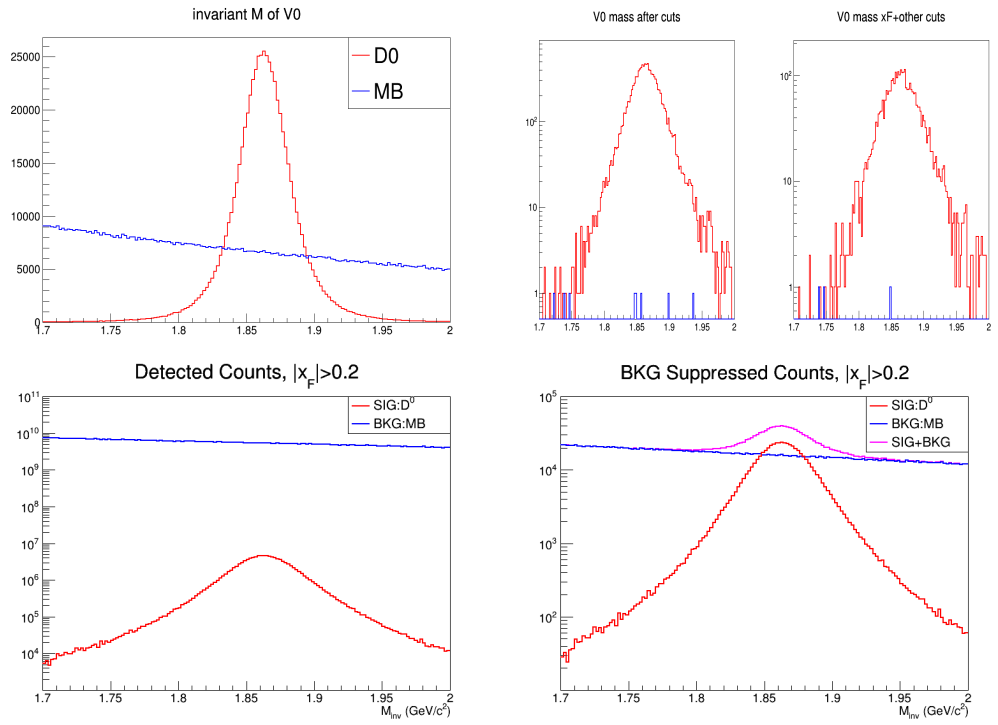

(a) Simulated invariant mass spectra (above), scaled to one year of data (below).

(b) Invariant mass spectra after selection (above), scaled to one year of data (below).

Figure 16: Invariant mass spectra of π^+K^- for the ideal simulation for D^0.

Information from the SPD conceptual design report (CDR) are used to scale the simulated invariant mass spectra to mass spectra expected from one year of recorded data (corresponds to 1 fb^{-1} integrated luminosity that's expected for $\sqrt{s} = 27$ GeV). Simulated count of $D^0 \longrightarrow \pi^+K^-$ are scaled to the CDR value of 520 million expected in one year data. Background are scaled by the ratio of min-bias events for one year data (3800 B) to the simulated min-bias event count.

To generate projected invariant mass spectra after selection, signal and background suppression factors form the analysis (using counts before and after application of selection cuts) are also used. Figure 16 show original invariant mass distributions from the simulation study as well as the scale/projected distribution for one year of recorded data.

Of particular note is the effect of the selection criteria. As the 16a bottom

plot in Figure 16 shows combinatorial background from all hard (and soft) processes outnumber the D^0 signal by close to four orders of magnitude, illustrating the difficulty of making this measurement. However, the 16b bottom plot demonstrates the efficiency of the selection cuts to reduce the random background by multiple orders of magnitude, to the extent that in a limited range close the D meson mass, we retain more signals than background.

After selection the resulting invariant mass spectra are fitted with Gaussian signal and linear background. Width of the signal Gaussian is used to estimate signal and background counts within 2σ mass window and used to calculate the statistical uncertainties as described in section 4.

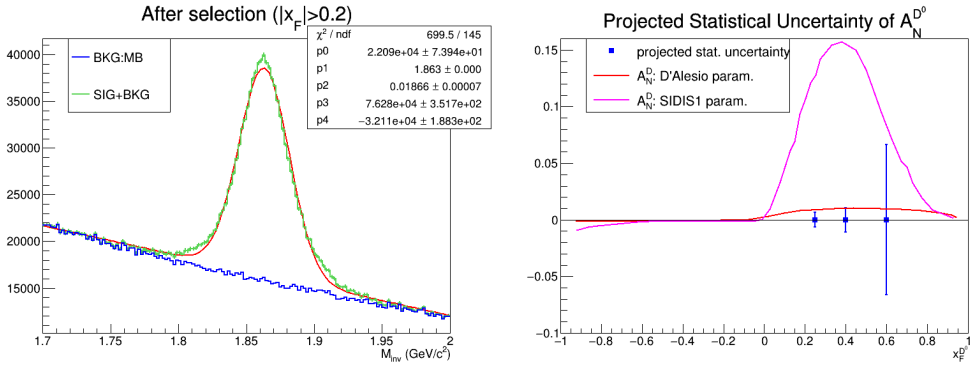

(a) Fit to the invariant mass spectra with a Gaussian signal and a linear background.

(b) Statistical uncertainties of $A_N^{D^0}$ in x_F bins compared to theoretical estimates for A_N of inclusive D

Figure 17: Impact of selection criteria expected $A_N^{D^0}$ precision for ideal simulation.

Figure 17b gives a tentative comparison of possible impact of neutral D meson TSSA measurements. For some ideal conditions, the measurements will most definitely be able to distinguish between two models of the Gluon Sivers Function (GSF) used in the illustrated inclusive D meson TSSA calculations [2]. However, in the next section we will delve into how this comparison evolves for a more realistic simulation.

5.2 Neutral D Realistic Simulation with MAPS 'wish-list' SVD

Next up, a more realistic simulation is performed. For this study, four million open-charm events are generated and as before all D^0's are forced to decay in the channel of our interest. Thirty million minimum bias events were generated to study the combinatorial background.

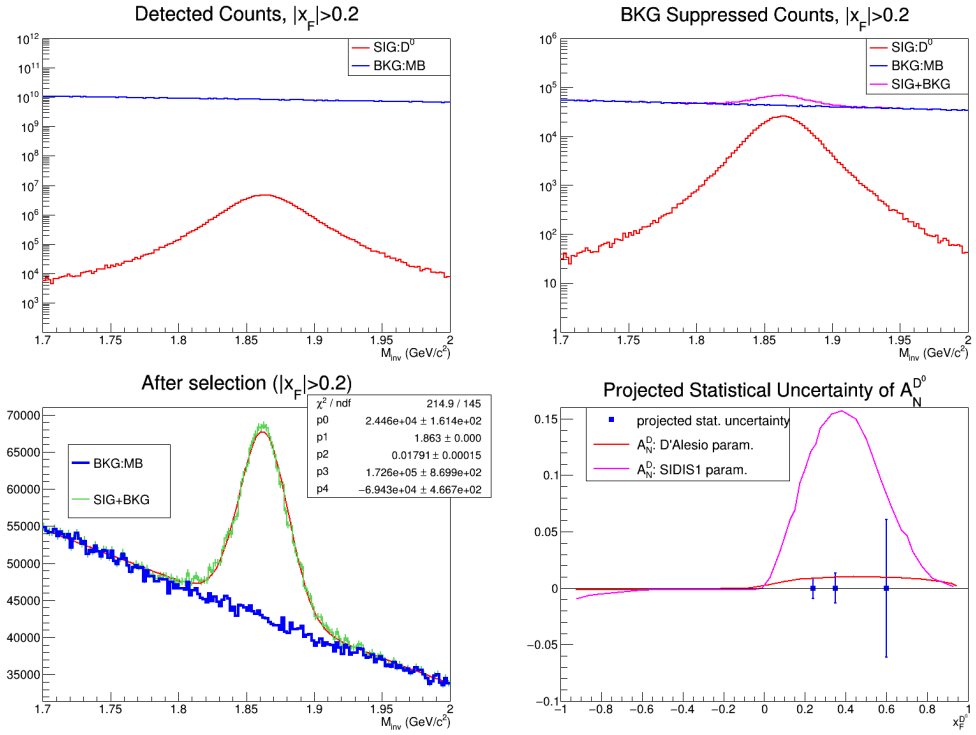

(a) Projected $\pi^+\pi^+K^-$ invariant mass spectra from one year data (above) fit to invariant mass spectra with Gaussian signal and linear background (below).

(b) Invariant mass for one year data after selection criteria are applied (above) and expected statistical uncertainty for $A_N^{D^0}$ compared to theoretical estimates for A_N of inclusive D.

Figure 18: Invariant mass spectra of π^+K^- for realistic simulation.

5.3 Charged D ideal Simulation with MAPS 'wish-list' SVD

Next, we studied charged D meson decay via hadronic decay channel and its reconstruction using daughter track candidates. Some methodological improvements were made. For example, many of the selection criteria were determined from the figure of merit (FOM $\frac{N_{sig}}{\sqrt{N_{sig}+N_{bkg}}}$) distribution. In rare cases i.e. for the collinearity angle that needs to be small based on kinematic and geometry considerations, cut was decides based on physics rather than the FOM.

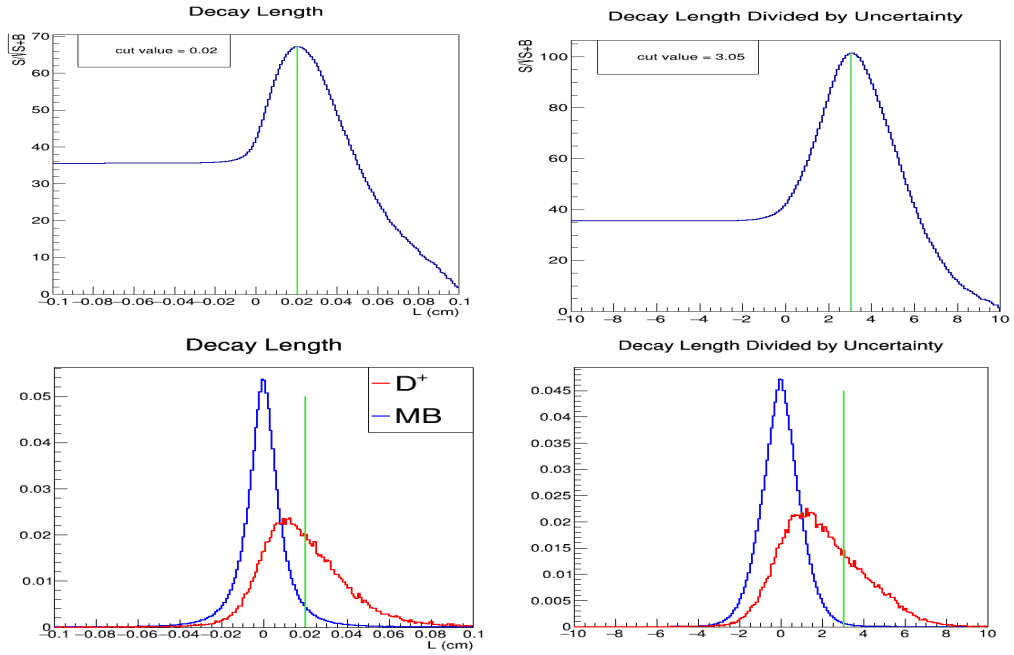

(a) D^+ decay length (figure of merit above).

(b) D^+ decay length divided by uncertainty (figure of merit above).

Figure 19: Example of figure of merit being used to decide selection criteria.

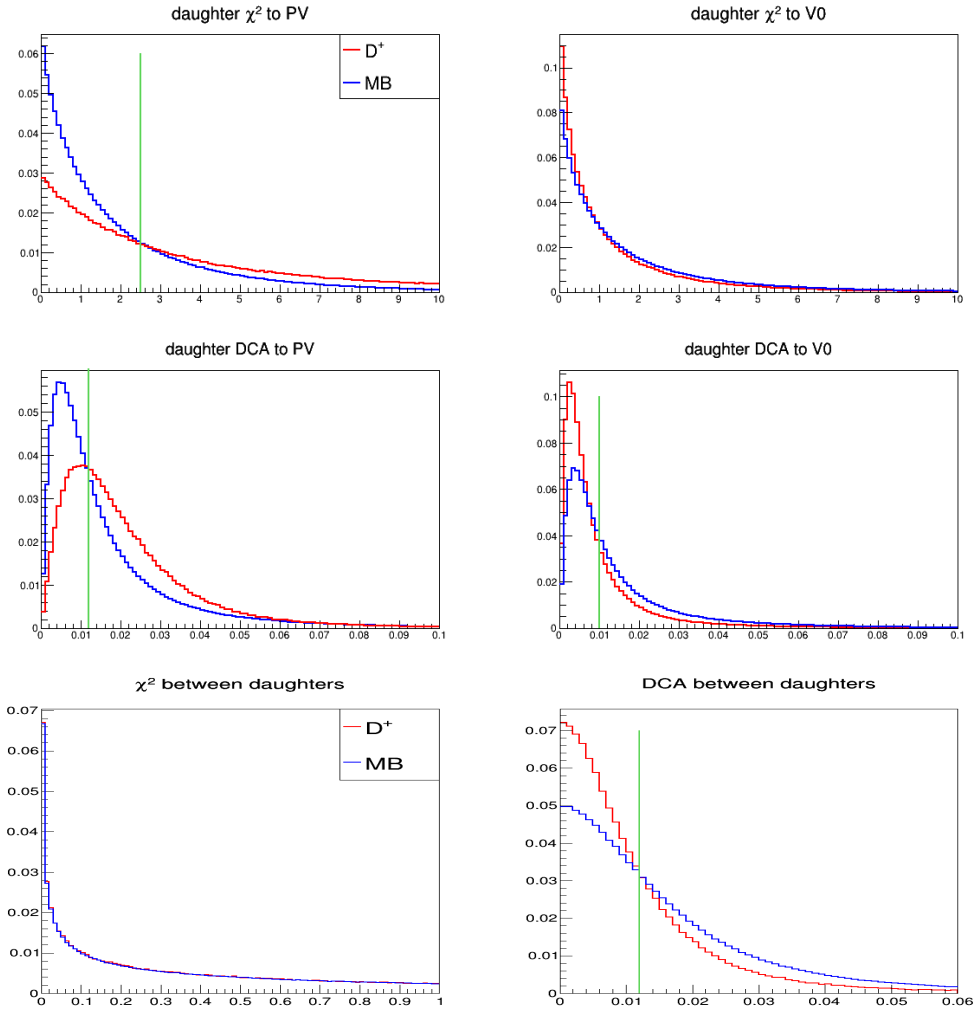

Figure 20: Daughter track properties. Cuts are shown with green lines.

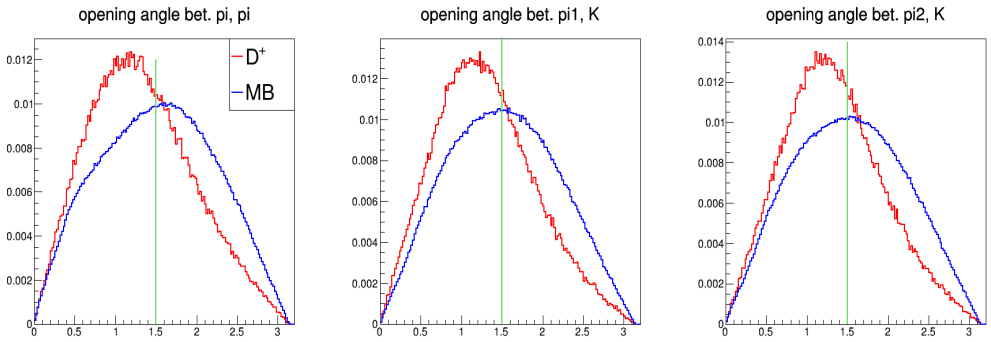

Figure 21: Opening angles between different pair of daughter tracks. Cuts are shown with green lines.

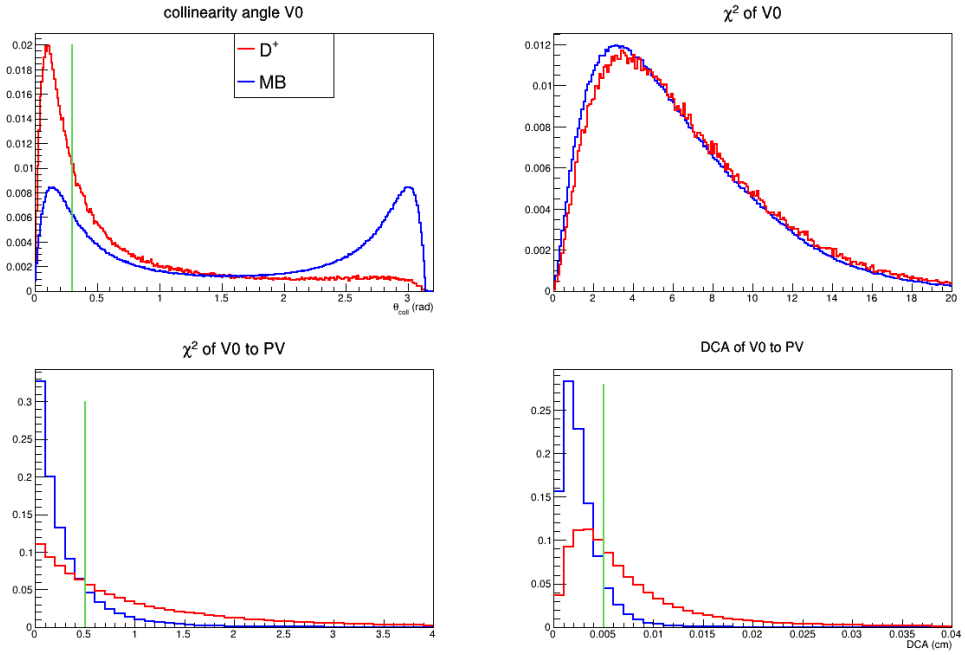

Figure 22: Properties of $\pi^+\pi^+K^-$ invariant particle. Cuts are shown with green lines.

Set of selection criteria for the simulated charged (positive in this case) D meson analysis are listed below :

- Decay length : $L > 0.02$ cm, $L/\delta L > 3.05$
- Collinearity angle : $Acol < 0.3$ rad
- V0 properties : $\chi^2_{V0-PV} > 0.5$, $DCA_{V0-PV} > 0.005$ cm
- Daughter track properties :
- $DCA_{\pi-K} < 0.012$ cm, opening angle $OA < 1.5$ rad
- Daughter to PV : $\chi^2_{d-PV} > 2.5$, $DCA_{d-PV} > 0.012$ cm
- Daughter to V0 : $DCA_{d-V0} < 0.01$ cm
- Invariant mass window 1.7-2.0 GeV/c^2
- $|x_F| > 0.2$ for asymmetry measurements

After selection, backgrounds are heavily suppressed and the resulting invariant mass spectra are fitted with a combination of two Gaussians for the signal and almost flat but in practice a very wide Gaussian was used to fit the background.

Weighted average of the two signal Gaussians is used as the effective mass resolution σ and this quantity is used to estimate signal and background counts within 2σ mass window which in turn are used to calculate the statistical uncertainties as described in section 4.

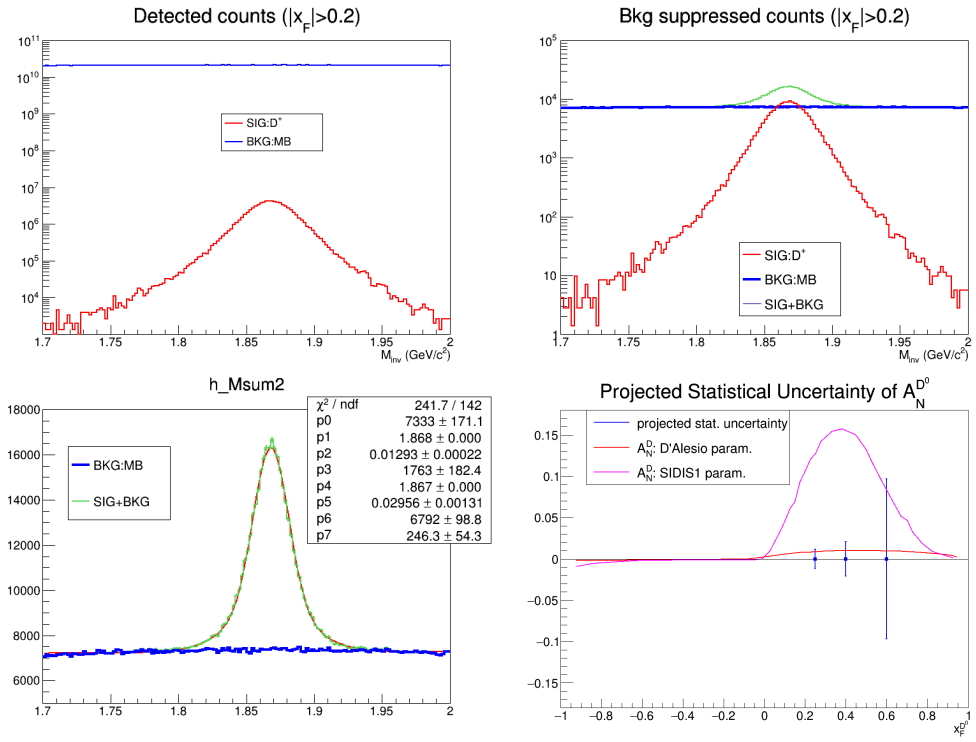

(a) Invariant mass spectra scaled to one year of data (above) and fit to spectra after selection with two Gaussians for the signal and a linear background (below).

(b) Invariant mass spectra, scaled to one year of data, after selection (above) and statistical uncertainties of $A_N^{D^+}$ in x_F bins compared to theoretical estimates for A_N of inclusive D (below).

Figure 23: Invariant mass spectra of $\pi^+\pi^+K^-$ for ideal simulation.

5.4 Charged D Realistic Simulation with MAPS 'wish-list' SVD

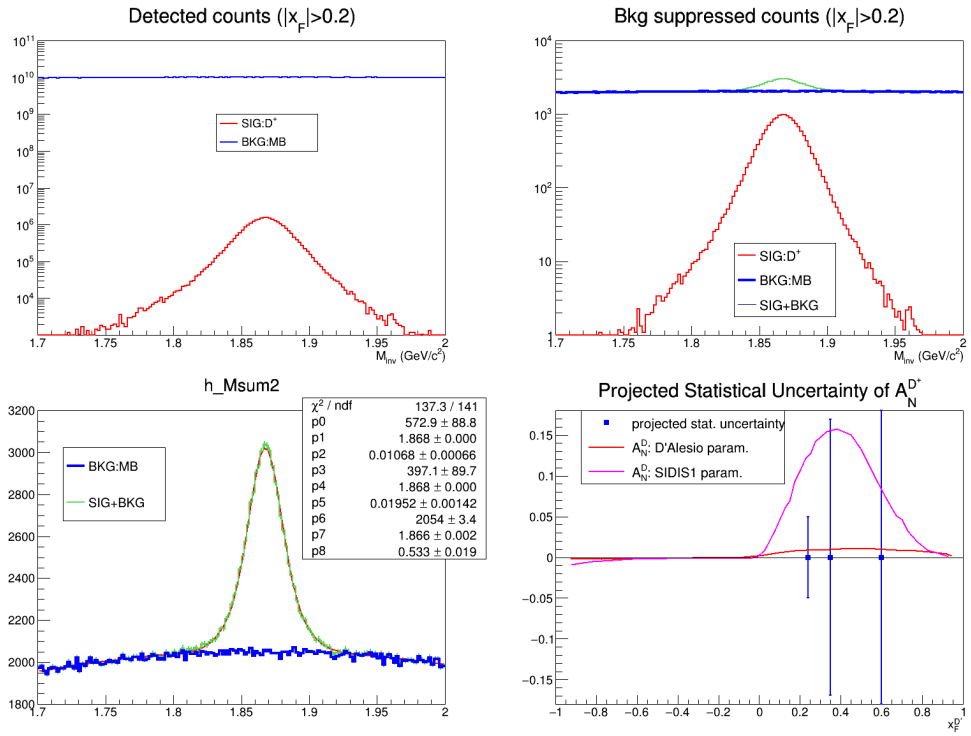

(a) Invariant mass spectra scaled to one year of data (above) and fit to spectra after selection with two Gaussians for the signal and a linear background (below).

(b) Invariant mass spectra, scaled to one year of data, after selection (above) and statistical uncertainties of $A_N^{D^+}$ in x_F bins compared to theoretical estimates for A_N of inclusive D (below).

Figure 24: Invariant mass spectra of $\pi^+\pi^+K^-$ for realistic simulation.

As figure 24 illustrates, in a more realistic situation, charged D meson reconstruction is significantly worse compared to an ideal condition of perfect PID (figure 23). As the number of daughter particles increase, so does the chance of mis-identification, resulting in a smaller number of signal compared to the ideal condition. This, again points to the importance of high accuracy and high precision particle identification required at the SPD for impactful charm meson transverse single spin asymmetry measurements.

5.5 Neutral D Ideal Simulation Without SVD

Four million open-charm and forty million minimum bias events were simulated without any (silicon) vertex detector. Perfect PID was assumed to study the effect of the lack of SVD. As the purpose of the SVD is to reconstruct secondary vertex with high precision (a few tens of micrometers), lack of this detector takes away our ability to reconstruct charm meson decay with any meaningful precision. Resolution of secondary vertex reconstruction is ~ 1 mm without any SVD.

As a direct result, almost all the quantities related to the secondary vertex reconstruction i.e. decay length (figure 25), χ^2 and DCA all become unreliable as distinguishing feature between the signal and the background. Of necessity one has to use kinematic quantities of the invariant particle and daughter track candidates to try to suppress background distributions, inevitably affecting signal (D^0 in this case) x_F distribution itself.

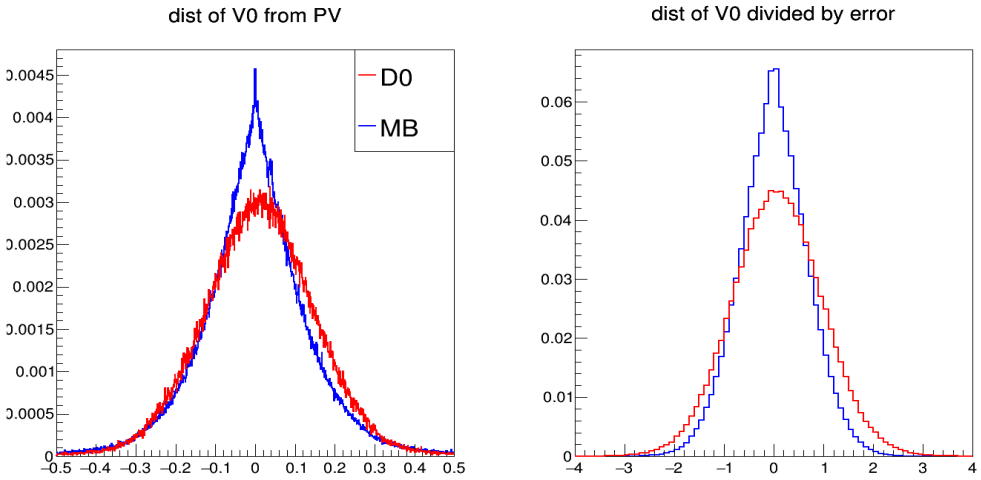

Figure 25: Decay length and uncertainty without SVD. Distinguishing features between signal and background are washed out.

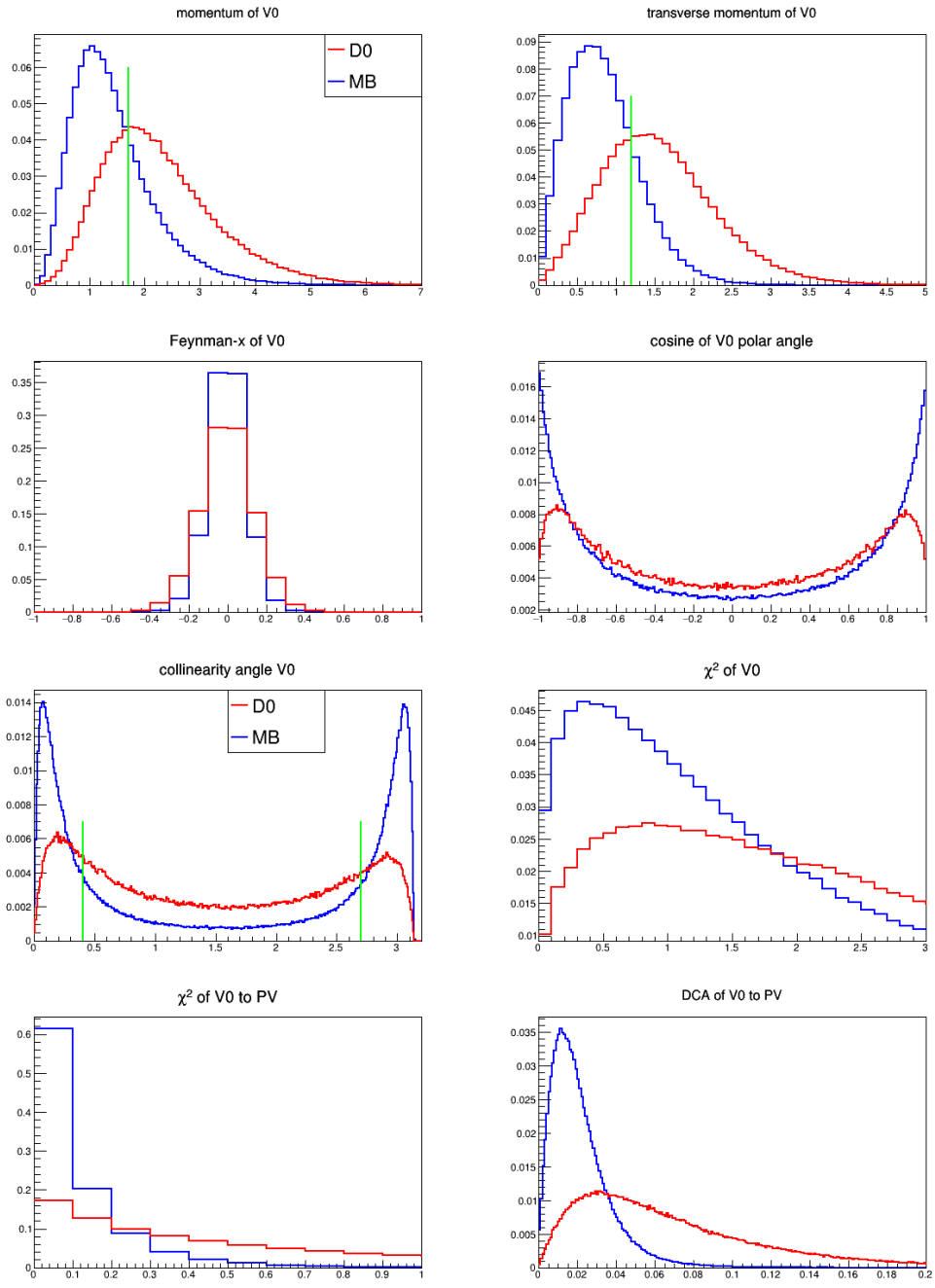

Figure 26: Quantities related to the π^+K^- invariant particle. Selections are based on some kinematic variables. Shown with green lines.

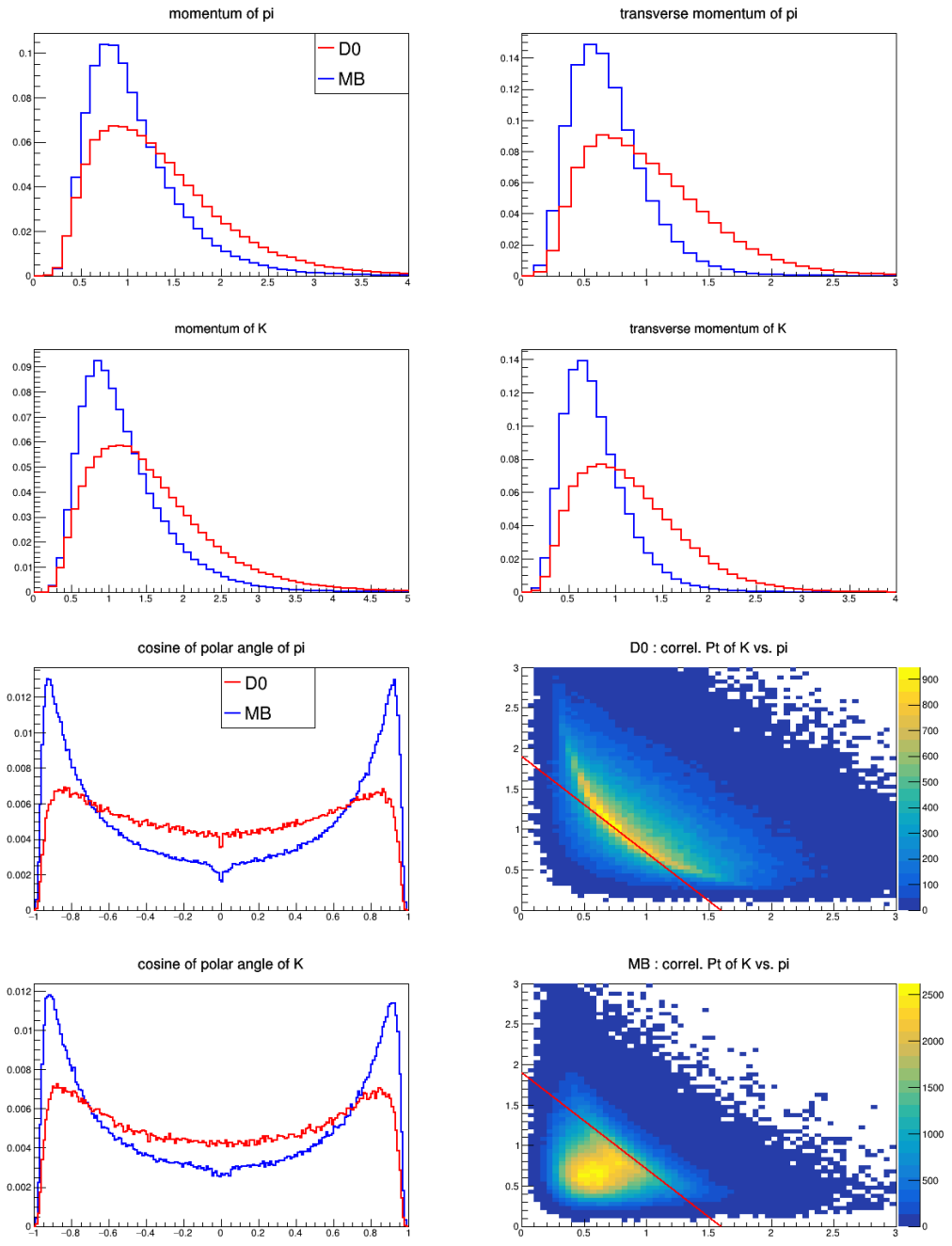

Figure 27: Daughter track candidate kinematic properties. Cut applied to pion-kaon correlated transverse momenta distribution (bottom right).

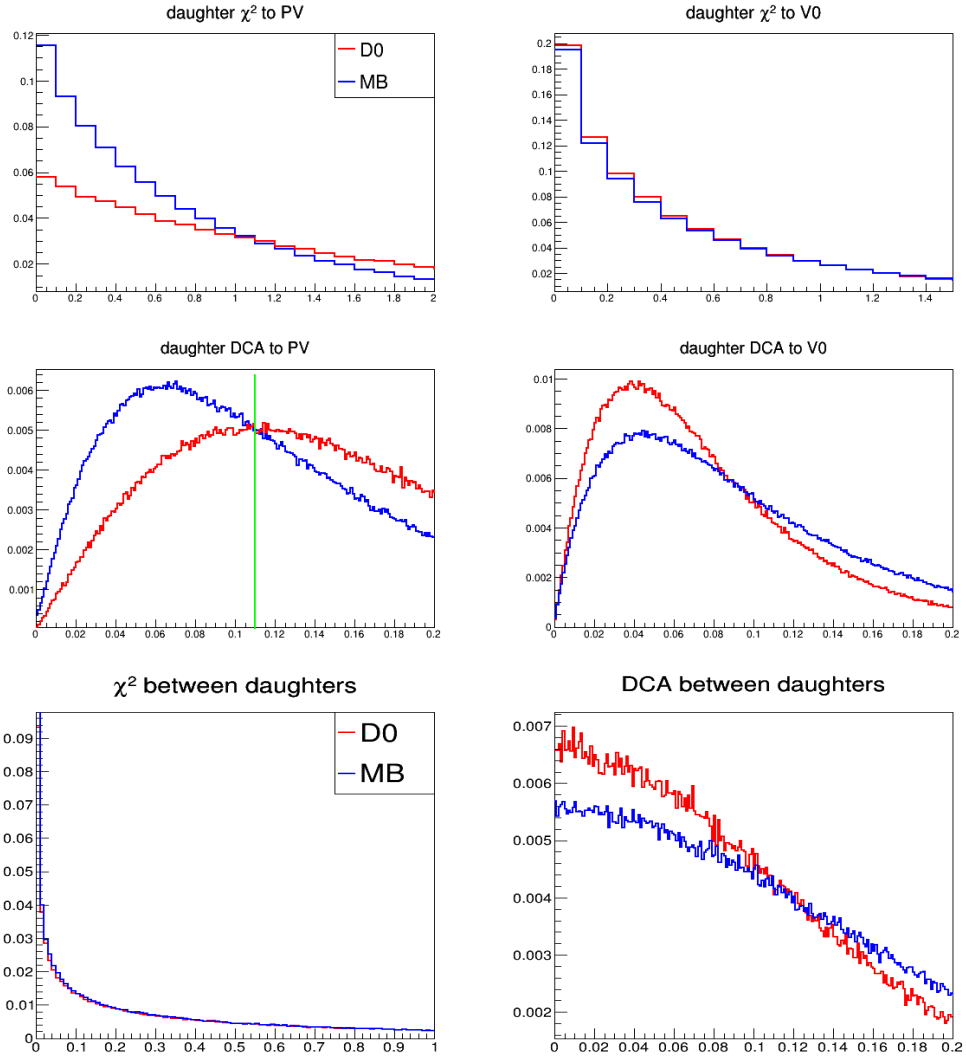

Figure 28: Daughter track candidate properties related vertex reconstruction. Most are not useful without the presence of SVD.

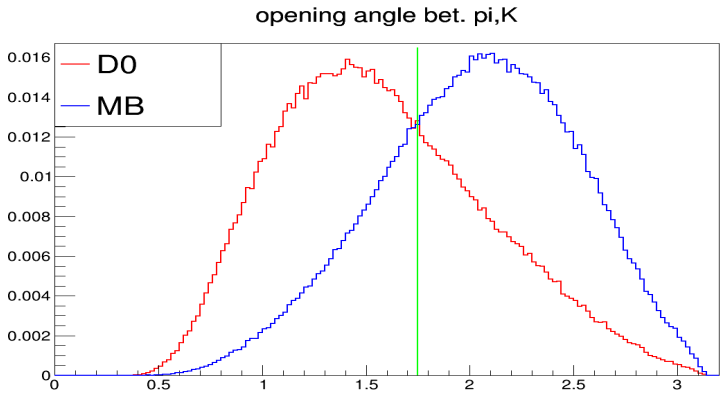

Figure 29: Opening angle between the daughter tracks.

Full set of selection criteria are listed below :

- V0 properties :
- Collinearity angle : $0.4 \leq Acol \leq 2.7$ rad
- $p^{V0} > 1.7$ GeV/c and $p_T^{D^0} > 1.2$ GeV/c
- V0 to PV : $DCA_{V0-PV} > 0.035$ cm
- Daughter track properties :
- Opening angle $OA < 1.75$ rad
- Daughter to PV : $DCA_{d-PV} > 0.11$ cm
- Daughter to V0 : $DCA_{d-V0} < 0.09$ cm
- correlated daughter pT : $(1.9p_T^{\pi} - 1.6p_T^{K}) > 3/04$
- Invariant mass window 1.7-2.0 GeV/c^2
- $|x_F| > 0.2$ for asymmetry measurements

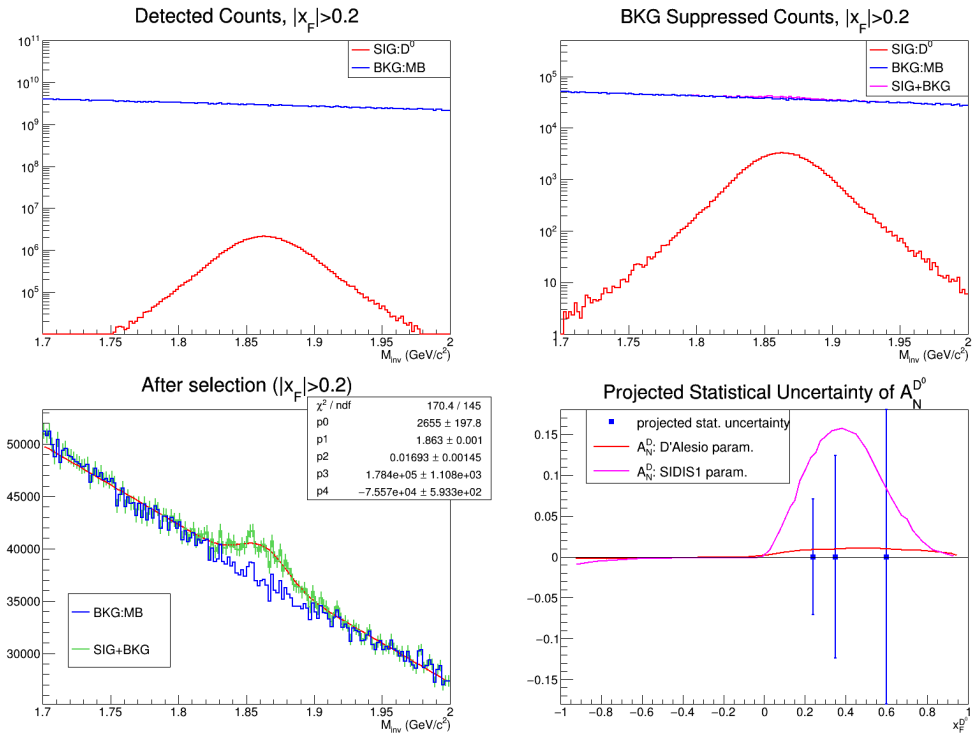

(a) Invariant mass spectra scaled to one year of data (above) and fit to spectra after selection with a Gaussian signal and a linear background (below).

(b) Invariant mass spectra, scaled to one year of data, after selection (above) and statistical uncertainties of $A_N^{D^0}$ in x_F bins (below).

Figure 30: Invariant mass spectra of π^+K^- for ideal simulation without any silicon vertex detector.

As the top plot in figure 30 b shows, the set of cuts is rather ineffective in suppressing background enough to be able to do a good fit of the resulting invariant mass spectra (lower plot in figure 30 a). Overall, this renders the TSAA measurement not very useful as it will not be able to separate between two models of GSF with meaningful confidence level.

5.6 Neutral D with MicroMegas

5.7 Neutral D with DSSD

6 Conclusions

References

[1] A. Guskov et al., *Conceptual design of the Spin Physics Detector*, **2021**, SPD CDR

[2] A. Arbuzov et al., *On the physics potential to study the gluon content of proton and deuteron at NICA SPD Prog. Part. Nucl. Phys.* **2021**, *119*, 103858.